Spring 5-2021

Characterization of the Sneathia amnii Cytotoxin and its Potential Role in Health Disparities Affecting Women of African Ancestry

Ivypel Amankwa-Asare
amankwaasare_i@lynchburg.edu

Characterization of the Sneathia amnii Cytotoxin and its Potential Role in Health Disparities Affecting Women of African Ancestry

Ivypel Obaapa Amankwa-Asare

Senior Honors Project

Submitted in partial fulfillment of the graduation requirements of the Westover Honors College

Westover Honors College

May 2021

_____

Jamie L. Brooks, PhD

_____

Ghislaine L. Lewis, PhD

_____

Beth Savage, PhD

Table of Contents

List of Figures

List of Tables

List of Abbreviations

Amp	ampicillin
B. pertussis	*Bordetella pertussis*
bp	base pair
BV	bacterial vaginosis
BVAB1	*Bacterial Vaginosis-Associated Bacterium 1*
BVAB2	*Bacterial Vaginosis-Associated Bacterium 2*
C-term	Carboxy- terminal domain
CptA	Cytopathogenic toxin A
ddH_2O	double-distilled water
DNA	Deoxyribonucleic acid
E. coli	*Escherichia coli*
EDTA	ethylenediamine tetraacetic acid
EMEM	minimum essential media
Fha	filamentous hemagglutinin adhesin
gDNA	genomic DNA
His	Histidine
IM	imidazole
IPTG	Isopropyl β-D-1- thiogalactopyranoside
kDa	kilodalton
L	Liters
L. crispatus	*Lactobacillus crispatus*
L. gasseri	*Lactobacillus gasseri*
L. iners	*Lactobacillus iners*
LB	Luria-Bertani
lbs	Pounds
Mb	mega base
ml	milliliter
mM	millimolar
MW	molecular weight
N-term	Amino-terminal domain
NIH	National Institutes of Health
nm	nanometer
OD	optic density
P. mirabilis	*Proteus mirabilis*
PBS	phosphate buffered saline
PBST	phosphate buffered saline supplemented with 0.05% Tween 20
PCR	polymerase chain reaction
PTB	Preterm Birth
PVD	pelvic inflammatory disease
PVDF	polyvinylidene fluoride
RNA	ribonucleic acid
RPM	revolutions per minute
rRNA	ribosomal RNA
S. amnii	*Sneathia Amnii*

SDS-PAGE	sodium dodecyl sulphate–polyacrylamide gel electrophoresis
Sn35	*Sneathia Amnii* strain 35
STD	sexually transmitted disease
TAE	tris-acetate-EDTA buffer
TPS	two-partner secretion
tRNA	transfer RNA
ul	microliter
UV	Ultraviolet
V	Volts
VCU	Virginia Commonwealth University
λ	lambda
°C	degrees centigrade

Abstract

Women of African descent are more likely to develop bacterial vaginosis (BV) and bear twice the risk of preterm birth and the increased risk of other pregnancy complications. *Sneathia amnii* is a pathogenic anaerobe found in the female urogenital tract that is associated with adverse outcomes such as preterm birth, BV, and chorioamnionitis. *S. amnii* has been found at a greater prevalence in the vaginal microbiota of women of African ancestry, which links it to a potential role in the disparities observed in health outcomes for these women. *S. amnii* encodes the cytopathogenic toxin A (CptA), an exotoxin that perforates fetal membranes and lyses red blood cells. This study seeks to determine which domain of the cytotoxin (N or C-terminal) is responsible for the cytotoxic and hemolytic activity. Our work has revealed that the C-terminal domain is involved in binding to some host cell surface receptors and that the N-terminal domain is the pore-forming domain. Our work also found evidence that the C-terminal binding domain can competitively inhibit the cytolytic activity of full-length CptA, which suggests that the toxin binds to a specific receptor and that binding is saturable. Advances in our understanding of CptA and *S. amnii* pathogenicity will lead to a more educated approach to therapeutic intervention and may reduce health disparities in gynecologic and obstetric complications associated with the vaginal microbiome.

Keywords: *Sneathia amnii*, hemolysis, rounding, cytotoxin, bacterial vaginosis, preterm birth

Introduction

I. Health Disparities in Research

Women of African are amongst people of minorities that are less likely to be included in research studies. Although National Institutes of Health (NIH) Revitalization Act dictate the inclusion of racial minorities in studies conducted in NIH-funded biomedical research, women of African ancestry continue to still be underrepresented in research pertaining to diseases/ conditions that particularly affect their lives (Chinn et al 2021). Conversely, representation of people of European ancestry continues to be prevalent in biomedical research (Bentley et al. 2020). This is troublesome as race and social factors influence the disease risk (Chen et al. 2014). Furthermore, women of African ancestry are at a higher disproportionate for health disparities as issues pertaining to them are either overlooked, and women of the European ancestry are set up as the standard for comparative analysis of disease risk. Therefore, based on data presented for white women as well as interventions set in place for them are use across the board to mitigate issues that affect subethnic groups.

Due to the lack of representation, women of African ancestry continue to face health disparities as they exist in limited research, therefore limited data about conditions that plague them and insufficient answers/ treatments to mitigate their problems proving detrimental to their health and mortality overall (Chinn et al. 2021). Furthermore, the lack of representation for women of African descent in research participation takes out the unique diverse perspective and conditions that can be studied, limiting the scope of understanding in research, and diminishing significant advancement to the field (Bentley et al. 2020). Thus, it is imperative to increase inclusion of minorities especially women of African ancestry to further understand human

biology, disease risks and to generate appropriate data that is truly representative of the population (Bentley et al.2017).

II. Healthy Vaginal Microbes and the Microbial Profiles of Women of African ancestry

A healthy vagina is colonized by *Lactobacillus* species that produce lactic acids to maintain the vaginal pH of less than 4.5 (Fettweis et al. 2014; Jefferson 2012). The acidity of the vaginal is essential for *Lactobacillus* species like *L. crispatus* to maintain a healthy microbial community in the vagina by secreting lactic acid, hydrogen peroxide, and bacteriocins to protect the vagina from colonization by other species (Jefferson 2012). The abundance of *L. crispatus*, one of the stable *Lactobacillus* species, reduces the competition of other species that are instable and pathogenic while *L. iners*, a less stable species, produce low lactic acid concentrations and are dominant in higher vaginal pH (Verstraelen et al. 2009; Jefferson 2012; Vaneechoutte 2017). Therefore, the reduction of various lactobacillus species reduces microbial protection against idiopathic diseases such as bacterial vaginosis, pelvic inflammatory disease (PVD), and increases the risk of experiencing preterm birth in women (Bayar et al. 2020; Jefferson 2012).

The microbial profiles of women of African American ancestry are more diverse because they are low abundance of *Lactobacillus* bacteria and have high diversity profiles of anaerobic pathogenic species (Fettweis et al. 2014). The abundance is relatively small in comparison to women of European ancestry because the vaginal samples of women of African ancestry their community is colonized with different dominant species of both *Lactobacillus* and anaerobic species (Fettweis et al. 2014). The vaginal microbial profiles of healthy nonpregnant women of African ancestry were populated with *L. iners, Gardenella vaginalis, Parvimonas, Mycoplasma hominis*, and anaerobes like *Sneathia, Porvetella species, BVAB1* and BVAB2, in comparison to profiles of women of European ancestry which were predominantly populated with *L. crispatus,*

L. iners, L. gasseri, Staphylococcus species and *Gardenella vaginalis* (Fettweis et al. 2014). These bacterial species put African American women two times more at the risk of dealing with negative pregnancy outcomes in comparison to women of European ancestry (Fettweis et al. 2014). Women of African ancestry compared to women of European descent are more likely to exhibit microbial diversity, and they are more likely to contract bacterial vaginosis (BV), which increases their risk for preterm birth (Fettweis et al. 2014).

III. Bacterial vaginosis

The known cause of vaginal inflammation and the disturbance of the vaginal microbiome is from bacterial vaginosis (BV) (Koumans et al. 2007). According to the National Health and Nutrition Examination Survey conducted from 2001-2004, BV is prevalent at 29.2% in women of all demographics within childbearing age (14-49), and 51.4% more prevalent in women of African ancestry (Koumans et al. 2007). Similar studies that supported the prevalence of BV in women of African ancestry reported that samples from women from ages 18 to 44 nonpregnant women of which, 330 women were of European ancestry and 960 were women of African ancestry, 22.8% of the African American women were diagnosed BV and only 6.5% in women of European Ancestry (Fettweis et al. 2014). The study also concluded that risk factors for BV include race/ethnicity, sexual partners, and in women with high frequencies of douching. Based on sociodemographic factors, BV prevalence as high as the sexual partners increased when looking at race (Koumans et al. 2007). BV is associated with many health risks including susceptibility of HIV and other STIs as well as with the rates of PTB seen in women of African ancestry. Pregnant Black women were more likely to experience adverse pregnancy outcomes like give birth prematurely due to the prevalence of recorded BV (Koumans et al. 2007). Thus, BV causes shifts in microbial community, which give rise to opportunistic microbes such as

Sneathia amnii, which appears to be innocuous in the uterine cavity but becomes pathogenic when the bacteria ascend the vaginal tract into the amniotic cavity.

IV. Preterm birth

Preterm birth (PTB), defined as a live birth less than the 37 weeks gestation period, is a universal health issue. Preterm birth is the major cause of the increase in neonatal mortality and morbidity rates worldwide (Giurgescu et al. 2013; Walani 2020). According to the PTB consensus from 2010, 184 countries, more than 25 million neonates are born preterm worldwide (Walani 2020). Similarly, WHO reports that a global estimate of 13 million–17 million births are preterm births with high rates, approximately 81.1% of these preterm births, occurring in South of Asia and sub-Saharan Africa (Chawanpaiboon et al.2018). Of the millions of preterm births worldwide, an estimated one million annual neonates deaths due to preterm birth complications (Walani 2020).

PTB is categorized into different gestational ages. Extreme preterm is classified by birth less than 20 weeks of gestation. Very Preterm Birth is noted by a gestation period more than 28 weeks but less than 32 weeks, and moderate-to-late preterm are births occurring between 32 weeks and 37 weeks (Jefferson 2012). Based on evidence from 67 countries, an estimate of 84.7% of PTB are grouped as moderate-to-late preterm births, and 11.3% are considered very preterm births. Only 4.1% PTB occur within less than 28 weeks gestation period globally (Chawanpaiboon et al. 2018). Of the estimate 15 million global score of annual preterm births, an estimate of 750,000 babies is considered extreme preterm deliveries (Walani 2020). Preterm birth neonates born less than 32 weeks and weigh less than 3.3lbs have lowest survival rates (Goldenberg et al. 2000).

V. Sneathia Amnii

Sneathia amnii is a newly recategorized anaerobe pathogen once classified under the *Leptotrichia* genus and was assigned the strain type named *Sn35* (Collins et al. 2001; Harwich et al. 2012). *S. amnii* was first isolated from mid vaginal samples of 736 women in outpatient clinics across the state of Virginia (Harwich et al. 2012). In past studies, *Sneathia* species including *S. amnii* was found in amniotic fluid collected from pregnancies associated with preterm labor (Han et al. 2009). Research hypothesizes that intrauterine infections and inflammations that are linked to preterm birth is through the ascension of pathogenic bacteria like *S. amnii* from the cervix into the placenta and fetal membranes as noted in diseases like chorioamnionitis where fluid from membrane rupture indicated the invasion of microbes (Jefferson 2012). This means that preterm-associated bacteria species like cross from the mother's side to the fetal side and causes intra-amniotic infections and inflammation that lead to preterm birth (Han et al. 2009).

According to recent studies, *Sneathia amnii* persists as a prevalent bacterial species in the urogenital tract of women of African ancestry (Harwich et al. 2012; Fettweis et al. 2019). Although *Sneathia* is prevalent in the human female vagina, it is understudied pathogen, which can also infect men (Gentile et al. 2020;). Additionally, due to the lack of abundant research on the bacteria and its role in the reproductive tract, there is hardly any published research about *S. amnii* infections outside the reproductive tract (Duployez et al. 2020). The presence of *Sneathia* in the uterine cavity is associated with negative pregnancy outcomes, perinatal and neonatal complications as well as obstetrics complications (Harwich et al. 2012). The complications include bacterial vaginosis, chorioamnionitis, amnionitis, preterm labor, stillbirth, and spontaneous abortions in pregnant women and women of childbearing age (Harwich et al. 2012).

It is also implicated in clinical conditions like PVD, infertility, salpingitis, and septic arthritis, and it is involved in neonatal and perinatal complications such as meningitis (Gentile et al. 2020) bacteremia. In men, it can lead to nongonococcal urethritis in men (Gentile et al. 2020).

Sneathia amnii is a gram-negative anaerobe with long-bacilli shaped morphology and rounded ends (Harwich et al. 2012). *Sneathia amnii* requires specific medium human blood for optimal growth and yields small flat colonies on blood agar in an anaerobic chamber (Gentile et al 2020; Duployez et al. 2020). Moreover, based on the study conducted as part of the Vaginal Human Microbiome Project at VCU. *Sneathia* species was determined as a predominant taxa in the vaginal microbiome (Harwich et al. 2012). The study derived this conclusion based on the abundance of *Sneathia amnii* identified by 16S rRNA analysis with more than 70% reads using a 0.1% abundance threshold and about 76.3% reads recognized as *S. amnii* presence in mid-vaginal samples, indicating its prevalence in the vaginal microbiome (Harwich et al. 2012). Furthermore, this bacterium is the smallest sequenced *fusobacteriacae* and its genomic size is approximately 1.34M base pairs with 1.2M bases making the DNA coding region (Harwich et al. 2012). Close analysis of the genome showed that the bacterium has a GC content of 28.3% and 852 genes associated with a putative function (Harwich et al. 2012).

S. amnii encodes an exotoxin, component A of the TPS called cytopathogenic toxin A (CptA), which has cytotoxic and hemolytic capabilities. Using this exotoxin, *Sneathia amnii* perforates membranes and lyses red blood cells (Gentile et al 2020). *S. amnii* genome contain tandem genes for encoding two-partner secretion system that allows CptA to be exported into epithelial cells to induce pore formation (Gentile et al. 2020). The bacteria's genome contains tandem genes that allow the secretion of the toxin via a Type Vb two-partner secretion (TPS) system delivering the toxin, CptA, into epithelial cells to form pores in plasma membrane and

induce osmolysis activity (Gentile et al. 2020). The Type Vb two-partner system is used by many fastidious gram-negative bacteria to transport virulence factors like hemolysins, endotoxins and other cytotoxins (Gentile et al. 2020). The two-partner secretion system has an effector coupled with a beta barrel transporter that forms in the outer membrane to delivers CptA into epithelial cells (Gentile et al. 2020). The CptA is the effector that the cognate transporter transports into the outer membrane of cells (Gentile et al. 2020). Based on in-silico analysis of the toxin, it shares similarities with well identified and studied region in Type Vb two-partner secretion system found in *Bordetella pertussis* named filamentous hemagglutinin adhesin (Fha). Based on the well-studied research about Fha, it is depended on its transporter, FhaC, to enter the outer membrane to form beta-barrel forming pores (Mazar and Cotter 2007). Additionally, the homology between CptA and Fha is 46% with only 261 aligned residues to CptA residues (Gentile et al. 2020).

VI. The exotoxin CptA

The toxin comprises of 1,881 amino acids and has an approximate molecular weight of 201kDA. It is a large protein, and the isoelectric point is 9.4 (Gentile et al. 2020). As mentioned previously, CptA is best modelled after Fha in *Bordetella pertussis* with only 29% identity and 46% similarity (Gentile et al. 2020). CptA toxin has two separable domains hypothesis to have independent functions – the amino-terminal domain (N-term) and the carboxy-terminal domain (C-term) (Fig. 1). The N-term of the CptA contain the CptA gene locus which encode the CptA protein that is responsible for pore-formation in cells (Gentile et al. 2020). The full length CptA is approximately 6300 nucleotides long (Fig. 1). The N-term domain is 3,978 nucleotides in length from the 5’ end of the *cptA* gene, and the C-term domain is 2370 nucleotides in length from the 3’ end of the *cptA* gene (Fig. 1). Based on analysis, the full-length CptA has a protein

size of 235 kDa. The amino terminal domain permeabilizes cells and has a protein size of 163kDa. On the other hand, the C-term is involved in binding to host surface receptors on epithelial cells and is made up of 6 consecutive tandem repeats of 80 amino acids. The C-term has protein size of the C-term is 99 kDa. There is little known about CptA and how it works.

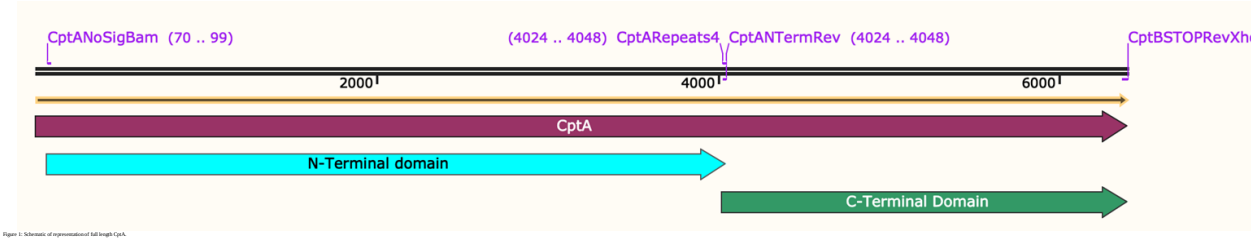

Figure 1: Schematic of representation of full length CptA and N-term and C-term domains of CptA. Shown is the amino-terminal domain and the carboxy-terminal domain with appropriate nucleotide length. Adapted from Dr. Jefferson.

VII. Research Objectives

Based on previous works, researchers have implicated *S. amnii* in gynecologic and obstetric complications associated with the vaginal microbiome. Furthermore, the exotoxin, CptA, encoded by *S. amnii* is known to perforate membrane cells and lyse red blood cells. There is little known about CptA and how it works. Therefore, advances in our understanding of CptA and *S. amnii* pathogenicity will lead to a more educated approach to therapeutic intervention and may reduce health disparities in women of African ancestry. Thus, the goal of this research is to discover CptA and its role in host-pathogen interactions by establishing and investigating the following objectives in this study:

1. Express the Full length CptA and the CptA domain peptides in *E. coli* cells and purifying them. Our work revealed that the peptides could be successfully expressed and purified.

2. Determine which domain of CptA is responsible for the cytotoxic and hemolytic activity. Our work has revealed that the C-terminal domain is involved in binding to the host cell surface and that the N-terminal domain is the pore-forming domain.
3. Identify the role of C-terminal binding domain in host-pathogen interactions. Our work found evidence that the C-terminal binding domain can competitively inhibit the cytolytic activity of full-length CptA, which suggests that the toxin binds to a specific receptor and that binding is saturable.

Materials and Methods

Culture conditions. The bacterial strain and plasmids used in this study are listed in **Table 1**. Bacterial strain used in this study was BL21(DE3) pLysS + pRIL *E. coli* cells. The *E. coli* strain was grown aerobically at 37°C on Luria-Bertani (LB) broth medium and agar plates containing 100ug/ml ampicillin overnight. *E. coli* grown in liquid cultures were incubated aerobically in LB broth at 37°C in an incubator shaker (Incubator Shaker Model G25 New Brunswick Scientific Co, Inc, Edison NJ) with heater for optimal oxygen supply to *E. coli* cells.

Table 1: Plasmid and bacterial strains.

Plasmid	**Description**	**Source**
pET32a	*E. coli* expression vector with T7 promoter, beta-lactamase gene for ampicillin resistance, and N-terminal Trx/S-Tag/6X-His tag	Novagen
pET32-NTerm	pET32 containing nucleotides 1-3,978 from the 5' end of the *cptA* gene.	Jefferson Lab
pET32-CTerm	pET32 containing nucleotides 3,979-6,349 from the 3' end of the *cptA* gene.	Jefferson Lab

***E. coli* strain**	**Description**	**Source**
BL21(DE3) pLysS + pRIL *E. coli cells*	Chemically competent cells derived from *E. coli* BL21 strain. The BL21 strain is protease deficient. DE3 phage provides T7 to drive gene expression. pLysS plasmid suppresses basal expression of T7 RNA polymerase until induction by IPTG. pRIPL plasmid contains extra copies of genes that encode tRNAs that are rare in *E.coli* but common in *S. amnii*.	Stratagene

Agarose gel. 1% agarose-LE gel in 1X TAE. Ethidium bromide was added to the solution before pouring. 6X loading dye was added to DNA samples. The gel was run at 100 volts in 1X TAE buffer for 35 minutes. After separation, the DNA fragments were visualized under UV light. DNA size was determined by comparing the DNA sample bands against λ/HindIII fragments.

Protein expression. The pET32a vector was used to express fragments of CptA proteins. Proteins were expressed from the pET32a plasmids through the T7 promoter (Fig. 2). An expression strain containing the pRIPL plasmid was used because certain codons, including *argU* (AGA, AGG), *ileY* (AUA), *proL* (CCC), *leuW* (CUA) are rarely used in *E. coli* but much more commonly found in the *cptA* gene from *Sneathia amnii*. The cells were inoculated in LB medium with chloramphenicol and ampicillin overnight and placed in a 37°C shaker (Brunswick Scientific Co.; Edison NJ). The cells were subcultured in 500 ml LB broth to mid-log phase at 37°C before pET32a vector with CptA fragment was added and incubated in the shaker (Brunswick Scientific Co.; Edison NJ) for 2 hours.

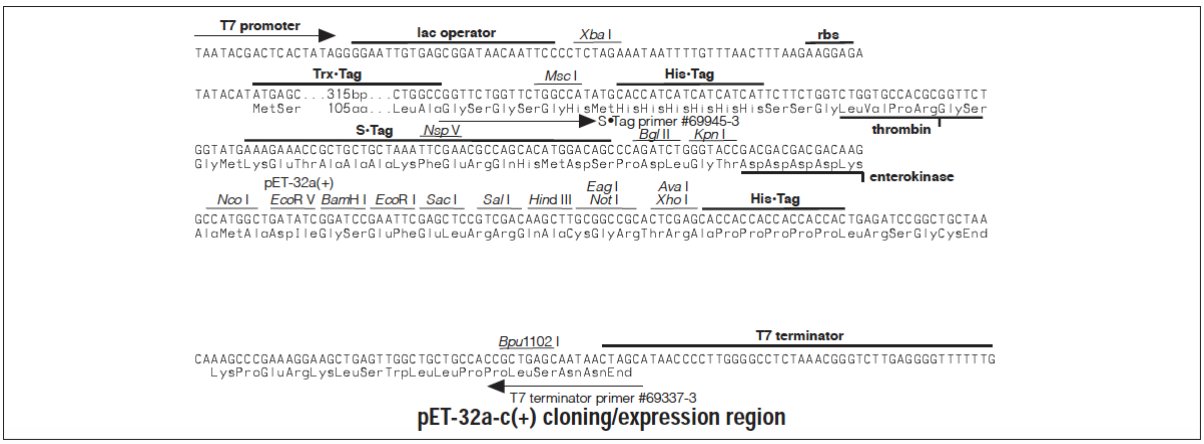

Figure 2: pET32a cloning plasmid expression vector.

Figure 2: pET32a cloning plasmid expression vector with T7 promoter, 6X His-Tag and the S-Tag. Figure 2 cited from Novagen (LaVillie 1993).

Polyacrylamide gel electrophoresis. Protein gels were run using the NuPAGE SDS-PAGE (Invitrogen). The running buffer for SDS-PAGE gel was prepared with 800 ml 1X MES running buffer consisting of 20 ml of MES SDS running buffer and 760 ml of ddH_2O. 10 ul NuPAGE 4X LDS Sample Buffer and 4 ul reducing buffer agent was added and mixed into 30 ul of sample. The samples were incubated in a heat block for 10 minutes, at 85°C and 20 ul of sample was loaded into the wells of NuPAGE 4-12% Bis-Tris 1.0 mm Gel. The gel was run at 200 volts in 1X NuPAGE Running Buffer for 30 minutes. Protein band size was determined by comparing the protein sample bands against BLUEstain protein ladder. After electrophoresis, the gel was washed twice with ddH_2O and placed on an orbital shaker to develop and for visualization.

Lysis of *E. coli* for the Purification of recombinant proteins. Protein was expressed in the BL21(DE3) pLysS + pRIL strain of *E. coli*. The frozen induced BL21(DE3) pLysS + pRIL + pET32a pellet was resuspended on ice with lysis buffer made using 250ml of 1X PBS and 100 mM NaCl (1.46 g) and one protease inhibitor tablet [cOmplete, EDTA-free protease inhibitor cocktail tablet] (Roche Diagnostics GmbH, Germany). The resuspended pellet was lysed with a French press 4 times. After lysis, the lysate was spun down in a centrifuge at 25000 RPM for 20

mins at 4°C. The supernatant was filtrated using a syringe capped with a pre-filter and a 0.45 um pore filter.

Protein Purification by Metal Ion Chromatography. The filtered protein was purified by nickel ion affinity chromatography. The purification column was prepared with 2.5 ml of Probond™ Resin (nickel beads) (Invitrogen Life Technologies Carlsbad, CA), which was washed with 11 ml of ddH_2O and equalized with 10 ml of 100 mM NaCl and 10X PBS buffer. The ProBond buffer was made with 25 ml of 10X PBS and 100 mM NaCl and detergent. The elution buffer was made with 250 ul of Ultra-Pure distilled water and 2.5 ml of 1M imidazole (IM). The filtered lysate was first added to nickel column and collected flow through for further analysis for cytotoxicity. The lysate in the resin column was washed 4 times with probond buffer, and the column was eluted with elution buffer. The column was eluted with 2 ml of dilution of imidazole at 1 M, 500 mM, 250 mM and 125 mM. At each step of the protein purification protocol, 50 ul aliquots of each step were saved in -80°C for further analysis. This procedure was done in a cold room. The same procedure was done performed with C-term fragment. SDS-PAGE Electrophoresis was performed with the saved aliquots to track the protein. The samples were prepared for SDS-PAGE using 50 ul of samples, 20 ul loading buffer and 7 ul reducing agent and heat in heat block for 10 mins. The 30 ul was loaded into each well as well as the 5 ul of molecular ladder. The gel was run for 30 minutes at 200V.

HeLa Cell Binding Assay and SDS-PAGE gel. HeLa cell monolayers were cultured in T25 flasks. The media was removed, and the HeLa cells were washed with 5 ml of PBS. Purified, recombinant N-term or C-term at a concentration of 5ug protein/mL in PBS or PBS alone, was added to T25 flasks 7 and the samples were incubated in 5% CO_2 incubator for 15 minutes. The cells were scrapped into 1 ml of SLS NuPAGE loading buffer (Invitrogen), sonicated for 30

seconds to break up DNA and put on heat block for 10 minutes at 85°C. Separate microcentrifuge tube containing either N-term or C-term peptides was mixed with a reducing buffer and put on a heat block with the rest of the samples. 20 ul of sample was loaded into each well of NuPAGE 4-12% Bis-Tris 1.0 mm Gel. The organization of the well is listed below:

1. 5 ul MW size marker
2. 20 ul of cells alone with PBS
3. 20 ul of CptA/N-term alone
4. 20 ul of CptA/N-term + Hela cells
5. 20 ul of C-term alone
6. 20 ul of C-term + Hela cells

The SDS-PAGE gel was electrophoresed at 200V for 30 minutes.

Prepared the transfer buffer and protein transfer. Transfer buffer was made with 40 ml of 1X NuPAGE (Invitrogen) added with 610 ml of ddH_2O and 150 ml of methanol. A 0.45 um PVDF membrane (Invitrogen, Grand Island, NY) was pre-wetted in 100% methanol for 30 seconds to 1 minute. Transfer filter paper and sponges were soaked and saturated in the transfer buffer as well as the PVDF membrane was rinsed with transfer buffer for a few minutes. Following polyacrylamide gel electrophoresis, the gel was prepared for transfer by rinsing in ddH_2O and then placed against the PVDF membrane carefully to eliminate bubbles, which would inhibit the transfer of proteins. The gel and PVDF membrane were surrounded by the transfer filter paper and sponges to maintain buffer saturation and tight contact between the membrane and gel, and the same 1X NuPAGE transfer buffer. The SDS-PAGE electrophoresis gel was run for 1 hour at 35 volts.

Western blot to detect 6X-His-tagged proteins. The blocking buffer contained 5% skim milk diluted in 1 X PBS. The wash buffer was prepared using 1X PBS and 0.05% Tween 20 (PBS-T). The PVDF membrane was soaked in the milk blocking buffer made of 5% skim milk diluted in 10X PBS for 1 hour, while rocking on an orbital shaker at room temperature. The milk blocking buffer was removed and replaced with a 1:10,000 dilution of anti-6X HIS Tag primary antibody in PBS-T. The PVDF membrane was agitated on the orbital shaker gently for 1 hour. After the hour, the solution was poured out and the PVDF membrane washed three times for 5 minutes in 1X PBS-T. The PVDF membrane was probed with 1:10,000 goat anti-rabbit immunoglobulin-horseradish peroxidase conjugate (Invitrogen, Grand Island, NY) in 1X PBST for 1 hour at room temperature and rocked on the orbital shaker. The PVDF membrane was rinsed at room temperature with PBST three times for 5 minutes and once with ddH_2O. In the dark room, protein bands were developed using the saran wrap and ECL prime kit (GE Healthcare) to detect protein and measure the protein size. The blot was incubated in the chemiluminescence developing reagent for 1 minute, covered in saran wrap, exposed to X-ray film and developed in an X-O-Mat. The bands visualized were compared to BLUEstain protein ladder (Gold-Bio).

Cell culture. HeLa cells were cultured in a 5% CO_2 incubator at 37°C in minimum essential media (EMEM) (Quality Biological, Gaithersburg, MD). HeLa cells were viewed under an inverted microscope for more than 70% confluence. The old EMEM was aspirated off the HeLa cells and discarded. The cells were washed in PBS and aspirated. The adherent cells were then covered with trypsin and returned to the incubator at 37°C and 5% CO_2 for 5 to 10 minutes for the cells to dislodge from the surface of the flask. The EMEM cell media was added to the cells and resuspended. The cells were split 1:10 split of cells into a new T25 flask with 1 ml of cell and 9 ml of fresh EMEM cell media or 1:20 split with 4 ml of cells into 6 ml of fresh new

EMEM. The remaining cells were split into 12 well plates with 0.5 ml per well. The cells were incubated in a 5% CO_2 incubator at 37°C, and the cells were passed every 4 days.

Hemolytic Assay. The purified peptides were incubated with human erythrocytes washed in PBS for 2 hours at 37ºC. The liberated hemoglobin was measured by optical density at 405nm via spectrophotometry (Biomate 3 Thermo Electron).

Cytotoxic assay with terminal domains of CptA. Cytotoxicity and cell permeabilization were monitored using an inverted microscope (EVOS) (Life Technologies, Carlsbad, CA). Media was aspirated from the wells, and the cells were washed with PBS. PBS was added to each well, and 30 ul of N and C term peptides were added to HeLa cells and incubated in a 5% CO_2 incubator at 37°C for 2 hours. The cells were visualized, and images were taken with an inverted microscope EVOS AMEX-100 microscope (Life Technologies, Carlsbad, CA) to examine membrane permeability and cell morphology of HeLa cells. Trypan blue (Thermo Scientific, Waltham, MA) at 1:3 dilution was added to each cell and let to set for 2-3 minutes. The trypan blue was aspirated off the well and viewed under microscopy. The cells were analyzed using trypan blue exclusion method**.** The cytotoxic assay was repeated with saved aliquots from the purification steps.

Cytotoxic assay with terminal domains of CptA at different volumes. The cytotoxic assay performed on HeLa cells was done to monitor cytotoxicity and cell permeabilization under an inverted microscopy. The old media in the wells in the 24-well plate were aspirated, and the cells were washed with PBS. 250 ul PBS was added to each well with the exception of 500 ul added to the first column of well-plate. C-term was done with different volumes of C-term added to the 1st 2nd and 3rd row. 5 ul of C-term was added to the wells across the well plate in the first row.

In the second row, C-term was added at 0.5 ul volumes to each well in the second row and 0 ul in the 3rd row. The fourth row served as the negative control. 3 ul of CptA was added to each well in the first column and serial dilution was carried out by pipetting 250 ul across the wells. The HeLa cells were incubated in a 5% CO_2 incubator at 37°C for 2 hours. The cells were visualized under an inverted microscope to examine membrane permeability and cell morphology of HeLa cells. Trypan blue at 1:3 dilution was added to each cell and let to set for 2-3 minutes. The trypan blue was aspirated off the well and viewed under microscopy. The cells were analyzed using trypan blue exclusion method**.** The cytotoxic assay was repeated with different volumes of C-term and N-term.

In silico analysis. FASTA format sequence retrieved from NCBI was used to model the structure of toxin. The FASTA sequence of *Sneathia amnii* CptA document taken from Dr. Jefferson and ran that into n-BLAST. Based on Gentile et al. 2020, the CptA toxin was served for using command+F with keyword VC03_06090. The derived protein FASTA sequence for CptA was run in Phyre 2.0 software at normal mode using the sequence.

Results

The full-length CptA and the domains of CptA, N-term and C-term, were successfully expressed and purified.

The two domains of CptA, the structured amino-terminal, and the globular carboxy-terminal domain were cloned into pET32a expression vectors. The proteins were expressed in the BL21(DE3) pLysS + pRIL strain of *E. coli* cells. In Figure 3, full length CptA was purified by nickel ion column. Based on the SDS-PAGE analysis, the saved aliquots from the purification steps of CptA had faint bands appear at ~240 kDa. The bands did not appear when photographed, but when the gel was viewed physically, light band at ~240 kDa was seen in the 10 mM lane, but it was not captured on camera. The breakdown of the peptides appeared across all the columns with the different dilutions of imidazole. We expected a messy column for the lysate and less smearing for 500 mM IM.

In Figure 4, SDS-PAGE analysis was performed after purification of the full-length CptA and C terminal domain of CptA by nickel ion column. In Fig. 4, the proteins of the full length CptA and C-term domain were eluted from the nickel beads with 10 mM, 100 mM, or 250 mM imidazole. The proteins were seen for the C terminal domain at 98 kDa, and the full-length CptA was viewed at 235 kDa. The C-term domain was 80 kDa plus the 17.9 kDa tag. Similar to Fig. 3, the breakdown of the peptides was seen with the smearing of the bands. As expected, the smearing indicative of protein breakdown was seen in the flow through lane. It is our assumption that the breakdown of the peptides may be due to CptA protein being autocatalytic that is why we see the other bands appear. This hypothesis needs to be further investigated. Furthermore, due to the grand size of the domain terminal peptides, lack of separation of the peptides leads to

the smearing. The purified terminal peptides were eluted with and the bands were prominent. The peptides of C-term were seen at 98 kDa, and the full length CptA was viewed with bands at 235 kDa. In Figure 5, the purified domain peptides of C-term and N-term of CptA were visualized on SDS-PAGE gel after the peptides were eluted from the nickel beads with 10mM, 100 mM, or 250 mM imidazole. The C-term domain was 80 kDa plus the 17.9 kDa tag and the N-term domain was 145 kDa plus the 17.9 kDa tag. The bands appeared at 98 kDa for C-term domain of CptA and 163 kDa at N-term domain of CptA.

Both the N-term and C-term bound to HeLa cells

To investigate how the terminal domains of CptA interacted with HeLa monolayers, we added the purified domain peptides to HeLa cells and incubated for 15 mins. Then the cells were washed in PBS to remove the nonadherent proteins leaving the adherent within the HeLa cells. The cells were then sonicated to break up the cells and release the DNA and the samples for each adherent domain protein in the HeLa cells were run on an SDS-PAGE gel. The proteins were transferred to an PVDF membrane and was probed with both the primary antibody, anti-6X HIS Tag, and the secondary antibody, goat anti-rabbit immunoglobulin-horseradish peroxidase conjugate, and the bands were visualized by western blot. In Figure 6, the HeLa cells in the second lane served as the negative control and showed that the antibodies used for probing did not tag the proteins of the HeLa cells as indicative with no bands showing in the lane. Both the N-term or C-term peptides alone were added and served as positive control to show where the bands were supposed to appear. In Figure 6, in the N-term lane, we see multiple bands appearing in the lane. However, this is the only clearly the only visible bands present only in the N-term peptide alone lane with less lightly visible bands in the N-term bands added to HeLa cells and C-term peptide alone and absolutely no bands present in the C-term peptides added to HeLa cells. It

was our assumption that the malfunctioning of the western blot and the lack of inaccuracy of corresponding bands to the appropriate molecular marker of protein size was due to many possibilities including a lower concentration of the C-term peptide being added which although appeared on the SDS-PAGE gel, did not transfer to the PVDF, and was lost and that the N-term peptide concentration was twice as the concentration of the C-term peptide. Another possibility we considered was mutations in *E. coli* cells at the 6X His tag mutated from Histidine to proline, so the primary antibody was unable to probe the peptides. Thus, this was rectified in a second Western blot done by Mr. Jacob Raskind of VCU using an antibody for the S-tag as shown in Fig. 7. In Figure 7, the bands for the N-term peptide appeared appropriately around 240 kDa. However, a second was present, it was our assumption that maybe due to the autocatalytic nature of the toxin, it breaks down and the breakdown peptides were tagged.

Similar to the bands that appeared for the N-term peptides alone, the adherent N-term peptides in HeLa cells also had similar bands in the same range when compared to the N-term peptide alone bands. Furthermore, bands appeared for the C-terminal domain alone with smearing also present with the bands. Again, this may be due to peptide break down. However, the protein size of about 99 kDa was clearly visible in the lanes with the C-term peptides added to the HeLa cells. The appearance of bands in both the N-term added to HeLa cells and C-term added to HeLa cells lanes shows that both the N-term and the C-term peptides were adherent proteins and bound to HeLa monolayers. Additionally, in the western blot, the N-term and C-term were added to empty wells to test to adherence of the peptide to any surface. The lack of bands confirmed our assumption that the CptA's terminal domain peptides did not just adhere to any surface. Both the C-term and N-term were adherent to epithelial monolayer cells.

CptA N-term is hemolytic

We incubated the purified CptA peptide with human erythrocyte cells washed in PBS for 2 hours at 37ºC. The liberated hemoglobin was measured at optic density of 405 nm. In Fig. 8, N-terminal domain is hemolytic as a high absorbance was indicative of hemolysis seen at 500mM dilution with imidazole. N-terminal domain is hemolytic.

CptA N-term is cytotoxic, and C-term is not cytotoxic

In Figure 9, The N-term of CptA was cytotoxic and the C-term of CptA was not cytotoxic. In Figure 9A, N-term was capable of cell permeabilization and the N-term has an affinity for HeLa cell plasma membrane. The N-term permeated epithelial cells as noted by trypan exclusion. All the dead cells stained blue. In the HeLa cells in Figure 9B shows C-term added to HeLa cells. In Figure 9B, C-term did not permeate cell membrane as noted with less death. The C-term bound to some specific host cell receptors on HeLa monolayer cells. In the C-term, some rounding of the HeLa cells is noticed but not so much, as majority of the cells captured have their regular cell morphology that depict tear-shaped angular shaped with growth pattern of patchy monolayer.

C-term inhibited full-length CptA, possible competitive binding mechanism to some host surface receptor.

In Figure 10, C-term peptide to prevent full-length toxin-mediated cytotoxicity. When the N-term alone was added to HeLa cells, cell permeabilization was evidenced by trypan blue (Fig. 10). This supports our hypothesis that N-term peptides have an affinity for plasma membranes. We further discovered that when C-term was first added to the HeLa cells before the CptA, we discovered that the C-term inhibited the cell permeabilization of the HeLa monolayers. There were less cells stained with trypan blue. This lead and supports our hypothesis that C-term may

be participating in competitive binding kinetics to host surface receptors on HeLa cells and that binding is saturable.

In-silico analysis for protein structure of CptA

The results show homologous similarity of CptA structure to full-length FhaB in *Bordetella* as shown in Figure 11. The results also showed that the CptA sequence aligned to hemolysin in *P. mirabilis*. Based on in0silico analysis, 11% of the sequence (215 residues) was modelled with 100.0% to a highest scoring template. The proteins structure was modeled after template c3fy3A_ ranked #1, and it indicated the whole chain of the protein of modeled protein was a toxin, and the PDB molecule was hemolysin with crystal structure of truncated hemolysin a from p. mirabilis. The confidence level of the template c3fy3A_was 100, but the % identity was 26. Furthermore, based on analysis via the Phyre2.0 software, 772 residues (41%) could be modelled at >90% confidence using multiple-templates and 80% of CptA sequence was disordered and cannot be meaningfully predicted (Fig. 11). Furthermore, 3% of the sequence was alpha helix and 62% beta strands. A second hit was found with 100 confidence level for template d1rwra_ with a 29% identity. The second template matching to CptA sequence aligned with 261 residues, and this template was indicative of a domain of the protein. The template d1rwra_ characterized as a single-stranded right-handed beta-helix (Fig. 11). Additionally, the superfamily of the template d1rwra_ was Pectin lyase-like, and the family was Filamentous hemagglutinin FhaB, which is a secretion domain.

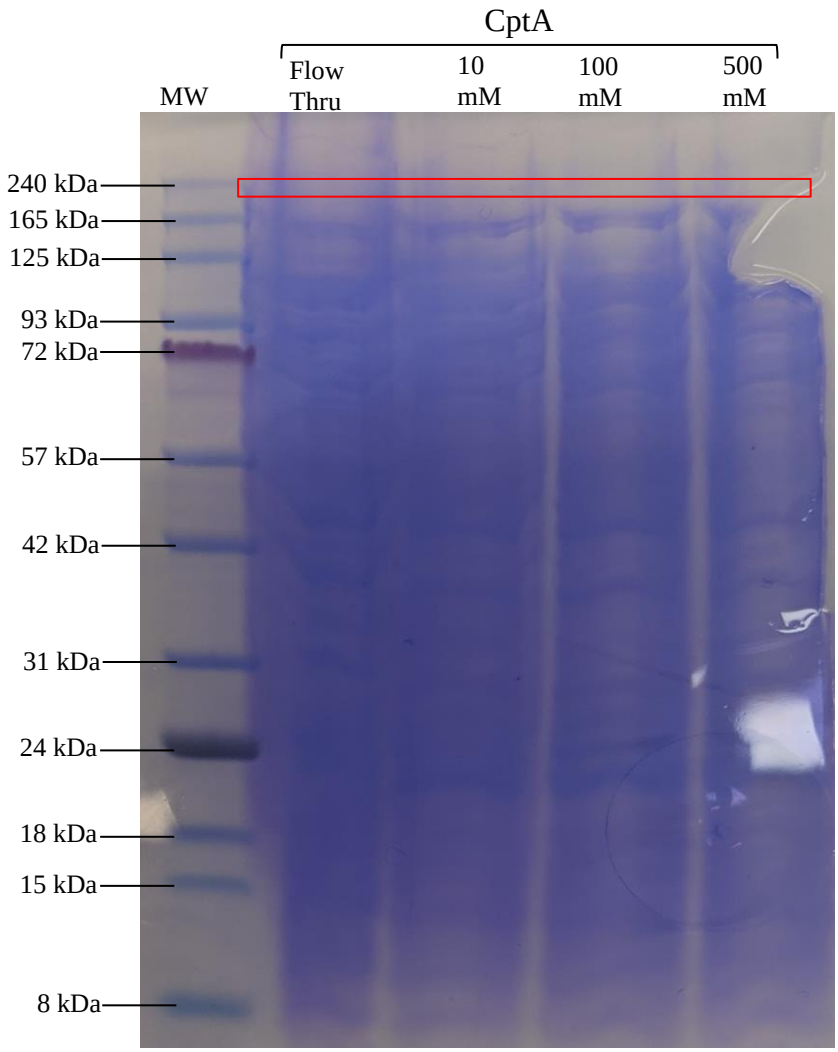

Figure 3: Purification of *S. amnii* full length CptA recombinant proteins. Purification of 6X-His tagged recombinant CptA expressed in BL21(DE3) pLysS + pRIL strain of *E. coli* cells containing pET32a using a nickel resin column. The samples loaded were compared against Blue stain protein ladder molecular weight in the lane 1. The SDS-PAGE gel shows the flow through lane in which the initial flow through was saved after passing the filtered lysate through the nickel resin beads in lane 2. The remaining lanes show the elution of the bound proteins with dilutions of imidazole. The lane 3 represents elution of the bound protein with Ultra-Pure distilled water + 10 mM imidazole. The lane 4 represented elution sample with dilution of 100

mM imidazole, and the lane 5 represented the sample with dilution of 500 mM imidazole. The protein size of CptA was indicated at ~240 kDa (235 kDa).

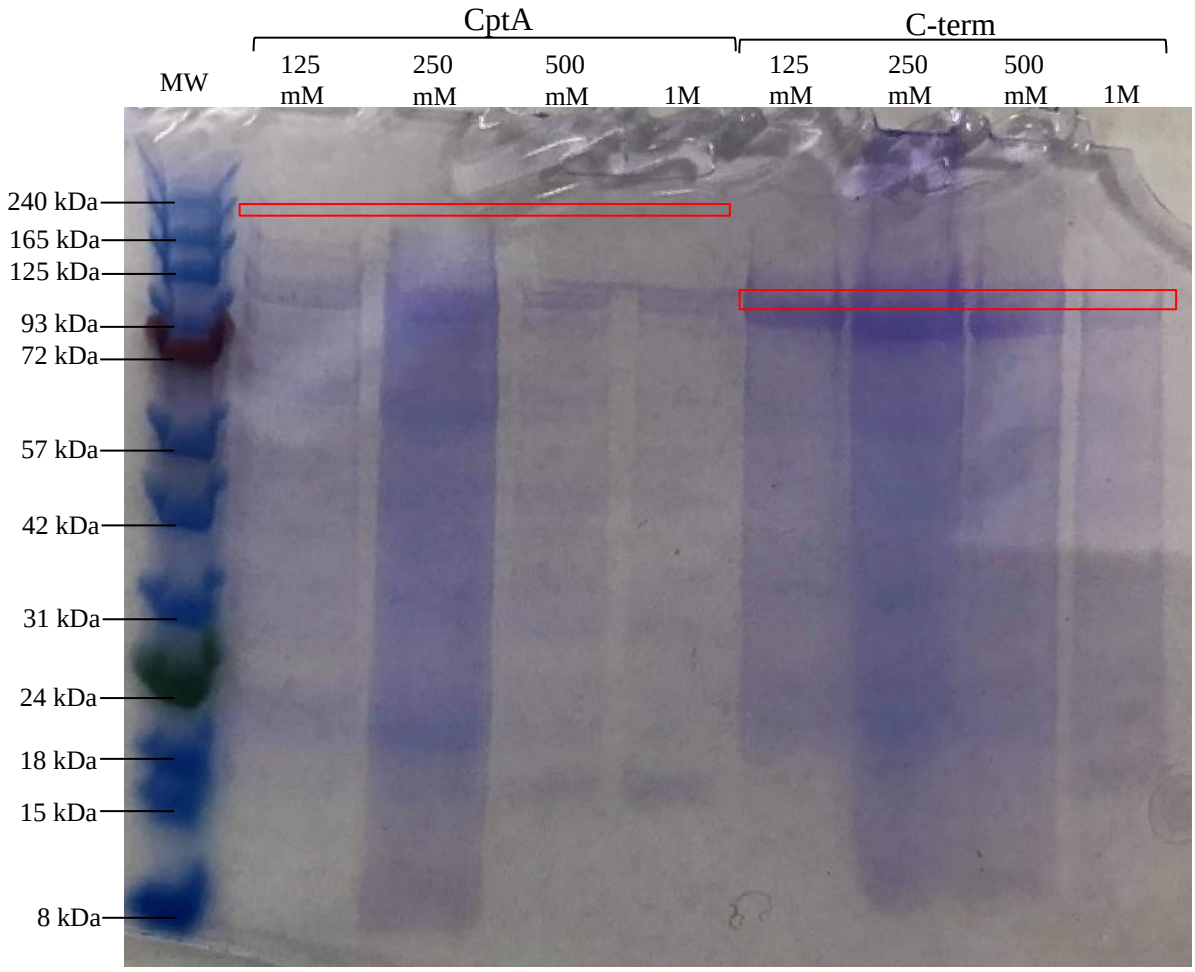

Figure 4: Purification of CptA CTerm (98 kDa) and full-length CptA (235 kDa). Purification of 6X-His tagged recombinant CptA expressed in BL21(DE3) pLysS + pRIL strain of *E. coli* cells containing pET32a using a nickel resin column. The samples loaded were compared against BLUEstain protein ladder molecular weight in the first lane. SDS-PAGE analysis of proteins eluted from the nickel beads with 125mM, 250 mM, 500mM or 1M imidazole for the both the N-term and the C-term. The protein size of full-length CptA was indicated at ~240 kDa (235 kDa) and the CptA's C-term domain was indicated at 98 kDa selected in red boxes.

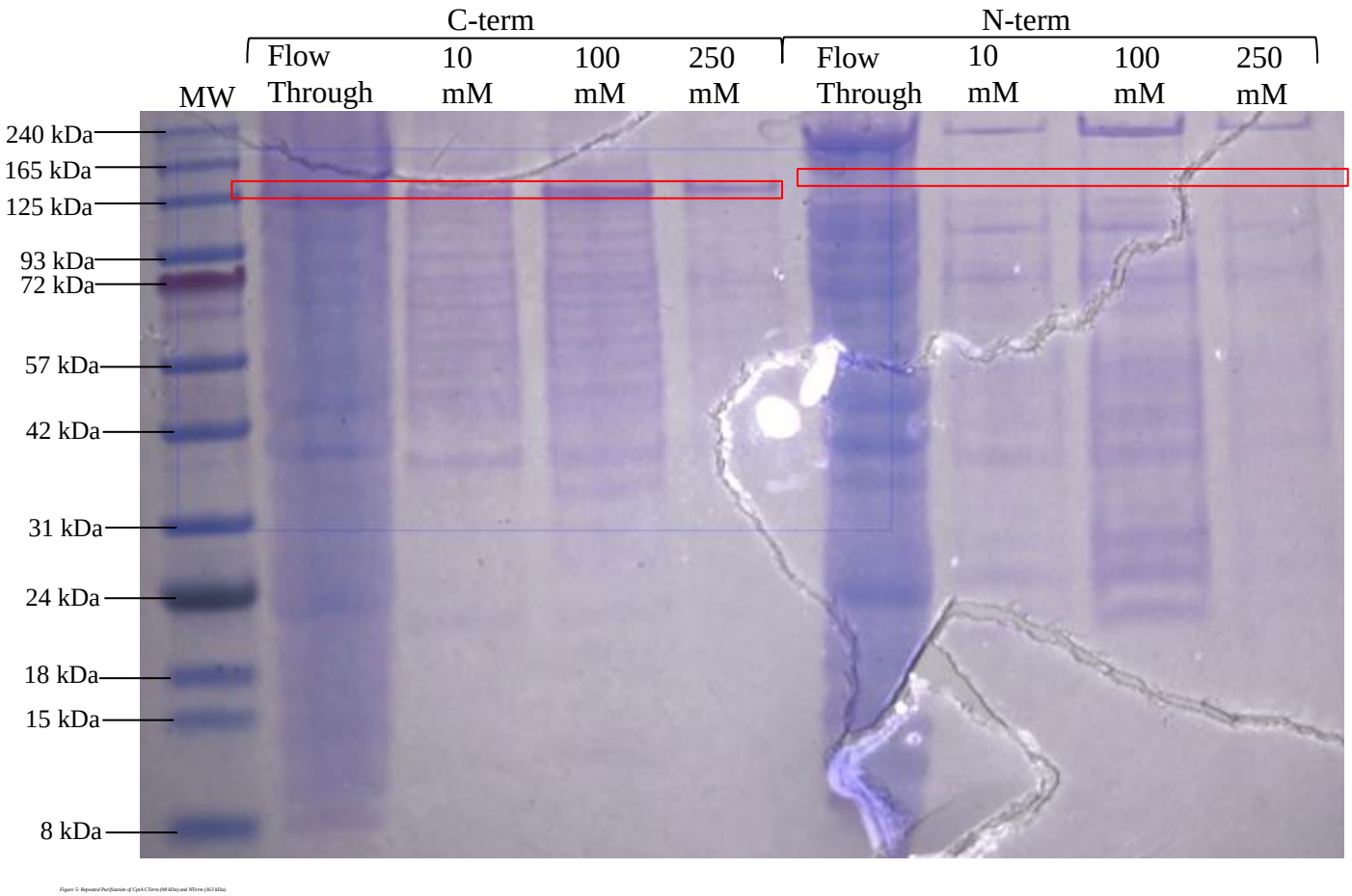

Figure 5: Repeated Purification of CptA C-term (98 kDa) and N-term (163 kDa). SDS-PAGE analysis of proteins eluted from the nickel beads with 10mM, 100 mM, or 250 mM imidazole. Approximate molecular weights are indicated from BLUEstain protein ladder compared to samples loaded.

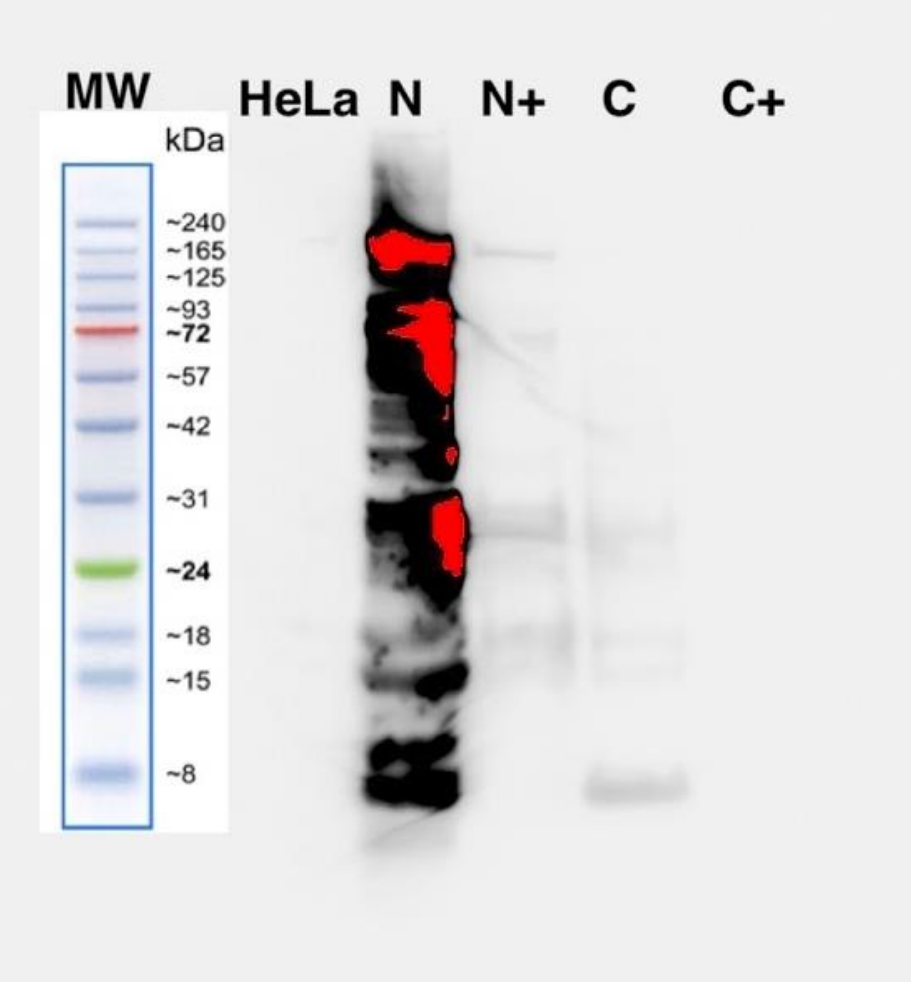

Figure 6: Adherence of CptA N-Term and C-Term peptides to HeLa cells.

Figure 6: Adherence of CptA N-Term and C-Term peptides to HeLa cells. Purified peptides were either added to HeLa monolayers for 15 minutes or developed as the peptide alone. The adherent proteins were developed by western blot. Approximate molecular weights indicated. Lane 1: HeLa cells alone; Lane 2: N-term peptides alone; Lane 3: N-term peptides added to HeLa cells; Lane 4: C-term peptides alone; Lane 5: C-term peptides added to HeLa cells.

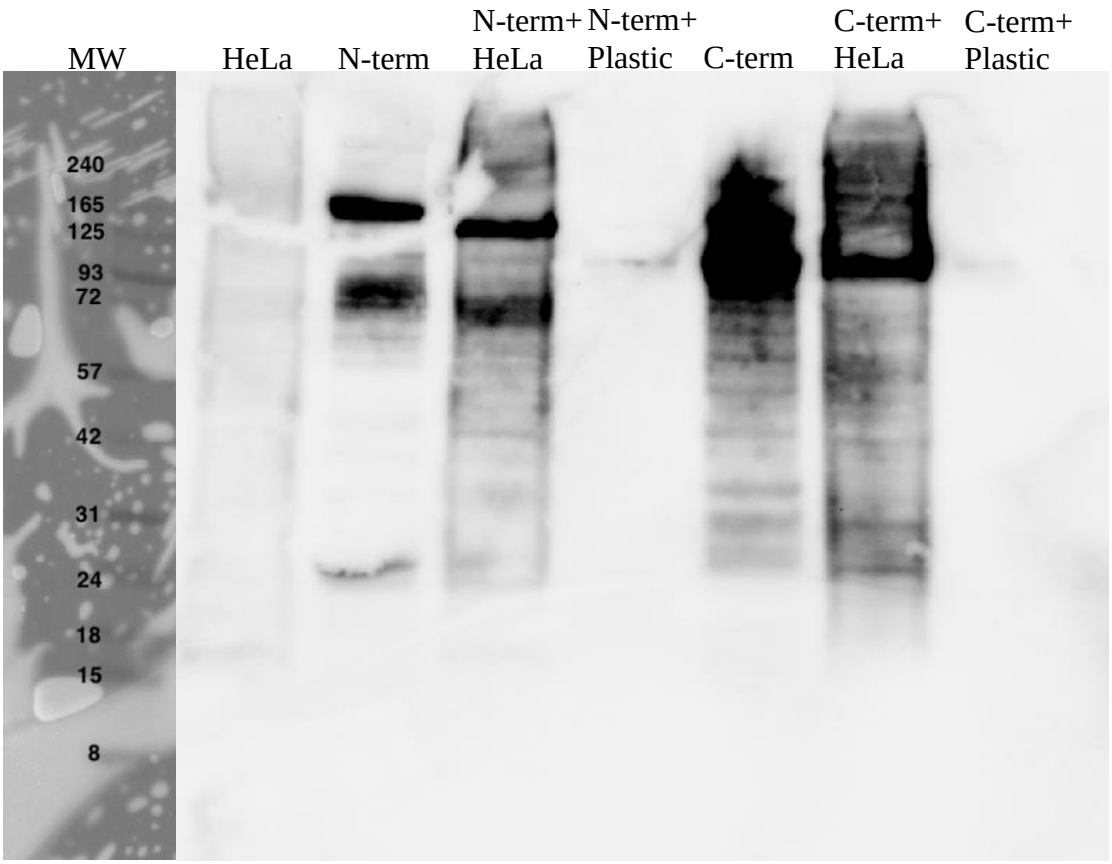

Figure 7: Both CptA N-Term and C-Term bind to HeLa cells. Purified peptides were added to HeLa monolayers or empty wells (bare polystyrene). Non-adherent protein was washed away, and adherent protein was detected by Western blot. Lane 1: HeLa cells alone; Lane 2: N-term peptides alone; Lane 3: N-term peptides added to HeLa cells; Lane 4: N-term peptides added to bare polystyrene wells; Lane 5: C-term peptides alone; Lane 6: C-term peptides added to HeLa cells; Lane 7: C-term peptides added to bare polystyrene wells.

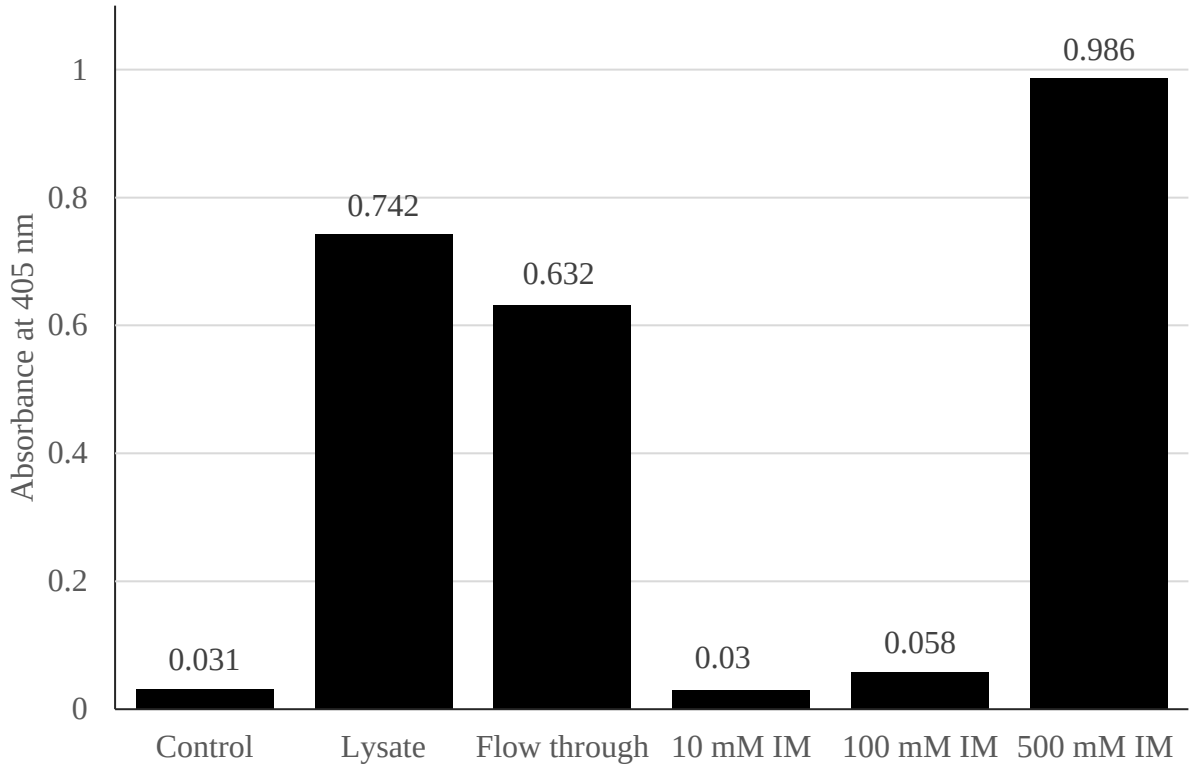

Figure 8: Full Length CptA hemolytic activity on human red blood cells. A hemolytic assay was performed by incubating full length CptA saved from the purification steps with human erythrocyte cells washed in PBS and incubated for 2 hours at 37ºC. The liberated hemoglobin was measured by optical density at 405nm.

A)

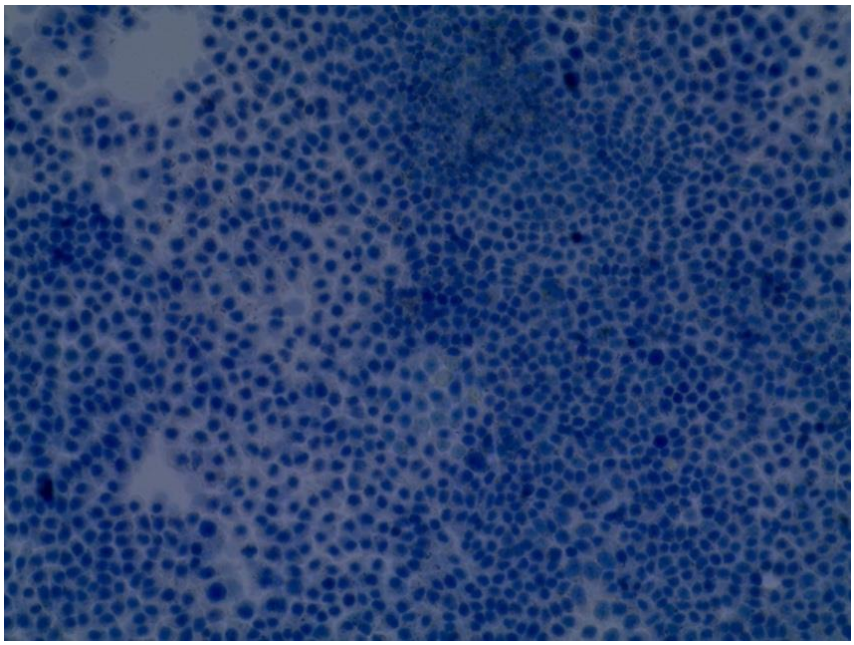

B)

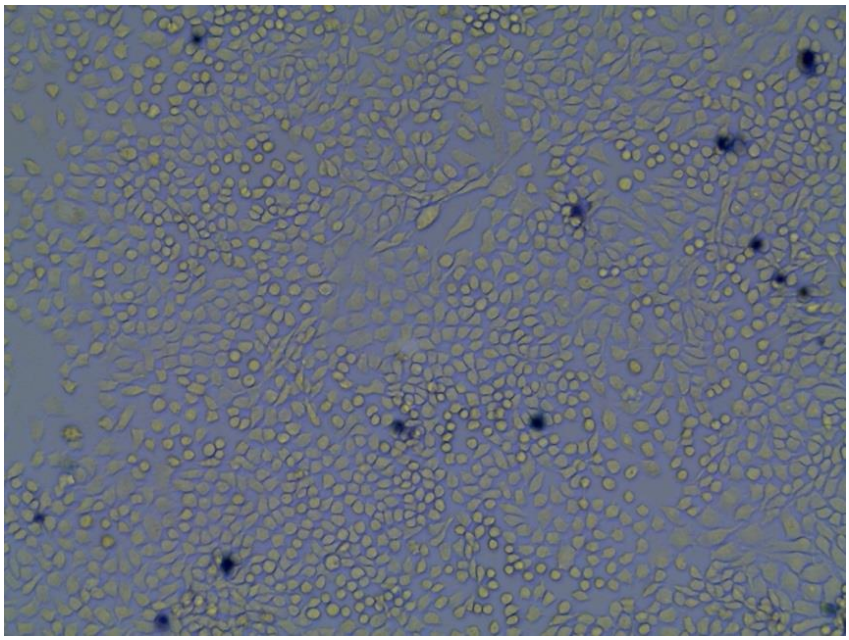

Figure 9: Cytotoxic assay using N-terminal and C-terminal domain of CptA

Figure 9: Cytotoxic assay using N-terminal and C-terminal domain of CptA. The HeLa monolayers were washed with PBS and incubated with the purified peptides in a 5% CO_2 incubator at 37°C for 2 hours. The cells were assessed using trypan blue exclusion and viewed under an inverted microscopy. Fig. 9A shows N-term/ CptA added to HeLa cells and Fig. 9B shows C-term added to HeLa cells. N-terminal domain has an affinity for plasma membrane.

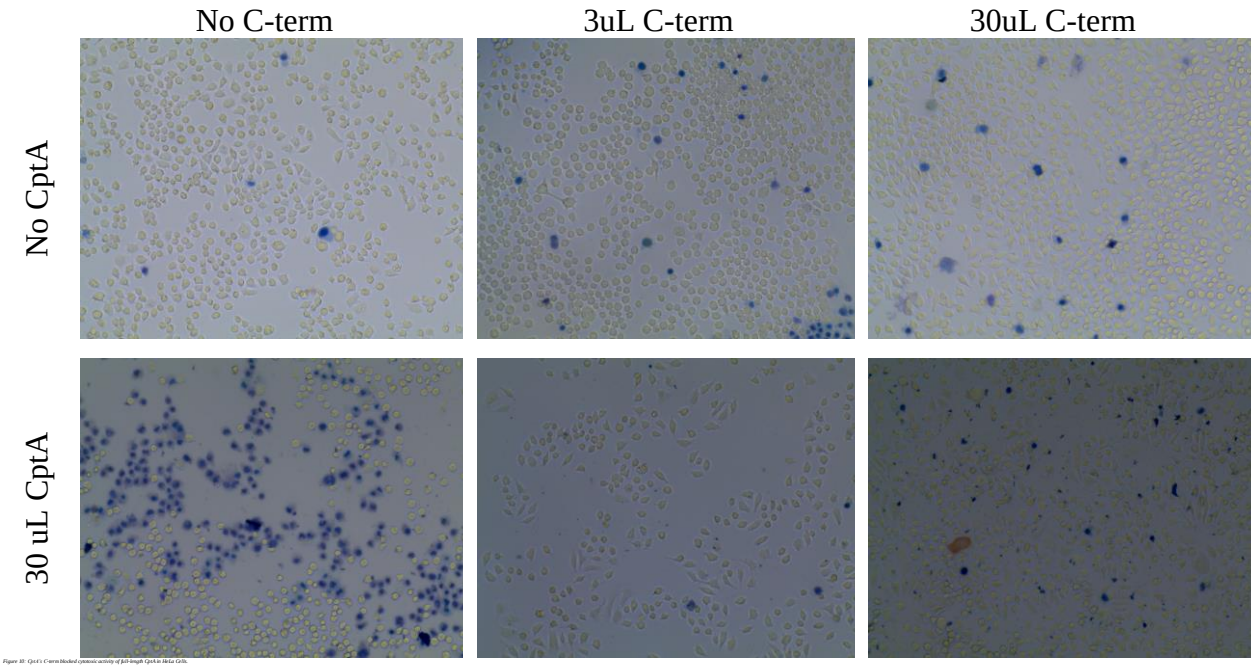

Figure 10: CptA's C-term blocked cytotoxic activity of full-length CptA in HeLa Cells. HeLa cells were washed with PBS and incubated with the purified peptides in a 5% CO_2 incubator at 37°C for 2 hours. The cells were stained with trypan blue exclusion and viewed under an inverted microscopy. C-term peptide prevented full-length toxin-mediated cytotoxicity.

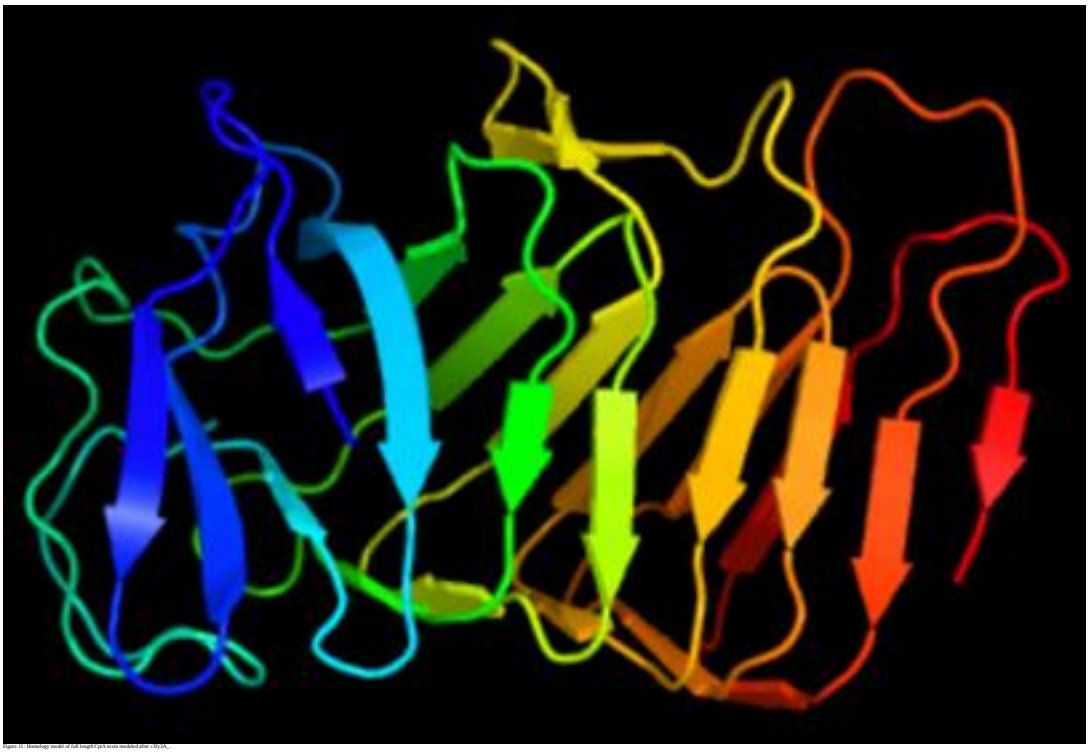

Figure 11: Homology model of full length CptA toxin modeled after highest score template c3fy3A_ using Phyre2.0 prediction protein modeling software. The template c3fy3A_ was a truncated protein from *P. mirabilis.*

Discussion

In the current study, we had the initial focus to characterize the CptA of *S. amnii*. The first research focus was to express the full-length CptA and the domains of CptA (N-term and C-term) in pET32a expression vectors in *E. coli* cells. It was hypothesized that *E. coli* cells could express the full-length peptides and domain peptides. This hypothesis was confirmed, as the SDS-PAGE gel analysis showed that the recombinant proteins were successfully expressed in BL21(DE3) pLysS + pRIL *E. coli* cells and purified by nickel ion column. In this experiment, we faced obstacles that included smearing of the proteins in the lane as well as the appearance of the other bands that were not the recorded protein size. While we were not able to determine the reason that the other bands showed up, we assumed that this may be due to the breakdown of the protein.

In the second objective, the focus of the study was to determine which domain of CptA is responsible for the cytotoxic and hemolytic activity. The data of this study contributes a clearer understanding of the roles of the CptA. We confirmed our hypothesis that CptA is hemolytic and that the N-terminal domain that codes for CptA was also hemolytic as it had an affinity for plasma membrane allowing the protein to perforate epithelial cell monolayers. While previous research (Gentile et al. 2020) has focused on CptA, these results of this experiment demonstrate that even the separable domains of CptA retain their function. Our work has revealed that the C-terminal domain is involved in binding to the host cell surface and that the N-terminal domain is the pore-forming domain. The results indicate that the C-terminal domain peptides was not cytotoxic and has a role in binding to some specific host cell receptor on epithelial cells.

Additionally, our findings supported the theory of full-length having hemolytic and cytotoxic effects on epithelial cells through in-silico analysis. Based on in-silico analysis of full

length CptA, it was reported that CptA was homologous with a small portion of a truncated hemolysin found in *P. mirabilis*. The in-silico analysis also matched a region of the secretion domain, Filamentous hemagglutinin (FhaB), in Bordetella species. Thus, the similar structural homology present supports in our Phyre 2.0 supports past studies that note that CptA toxin is secreted through a Type Vb two-partner secretion system where the effector, CptA which is homologous to Fha in Bordetella pertussis, is secreted by a transporter similar to FhaC in Bordetella pertussis.

In the third objective of this study, the focus was to characterize the role C-term plays in cytotoxicity. It was determined that C-term can prevent full-length CptA mediated cytotoxicity through competitive binding kinetics with some host cell surface receptors. Currently, it is not known what the host cell receptor in the protein-host binding interactions is. Therefore, further studies can be done to determine the specific host receptor as well as determine cytotoxicity over a longer period. Additionally, different epithelial cells can be used as model cell lines in the research. In future studies, C-term can be added first and incubated for a longer period to achieve saturation before CptA is added.

Other future works to advance the studies also include using CptA proximal binding partners on the target cells to determine structural protein composition via mass spectrometry to further understand how the toxin works and its function. Second, we can adapt methodology to determine the best way to purify the product with less breakdown protein. Lastly, further research can be done to design therapies to treat and prevent the prevalence of *Sneathia* species, which is common in the vaginal microbiome and prevalent in women of African ancestry.

Sneathia amnii has been implicated in gynecologic and obstetric complications associated with the vaginal microbiome. *Sneathia amnii* is categorized as a pathogenic anaerobe that

ascends the uterine cavity into sterile environments of the cervix and traverses epithelial cells to cross into amniotic fluid where it can be detected (Jefferson 2012). Although the specific role of *Sneathia amnii* is still being explored, our study has started to characterize the components of CptA and its role in idiopathic conditions like PTB and BV. *Sneathia amnii* is implicated in intrauterine infections and inflammations which are linked to preterm birth and prevalent in women of African ancestry (Jefferson 2012; Fettweis et al. 2014). Because women of African descent are more likely to develop BV, which is a gateway to more adverse outcomes including pregnancy complications. Studying *S. amnii*, its cytotoxin, and the role the bacteria plays in preterm-birth complication is essential in mitigating derived idiopathic conditions as well as reducing the overall rate of PTB as well as the health costs attributed to preterm birth deliveries.

References

Bayar E, Bennett PR, Chan D, Sykes L, MacIntyre DA. 2020. The pregnancy microbiome and preterm birth. Seminars in Immunopathology 42(4):487-99.

Bentley AR, Callier S, Rotimi CN. 2017. Diversity and inclusion in genomic research: Why the uneven progress? Journal of Community Genetics 8(4):255-66. doi: 10.1007/s12687-017-0316-6

Bentley AR, Callier SL, Rotimi CN. 2020. Evaluating the promise of inclusion of african ancestry populations in genomics. Npj Genomic Medicine 5(1):5. https://doi.org/10.1038/s41525-019-0111-x

Chawanpaiboon S, Vogel JP, Moller A, Lumbiganon P, Petzold M, Hogan D, Landoulsi S, Jampathong N, Kongwattanakul K, Laopaiboon M, and others. 2019. Global, regional, and national estimates of levels of preterm birth in 2014: A systematic review and modelling analysis. The Lancet Global Health 7(1):e37-46.

Chen MS, Lara PN, Dang JHT, Paterniti DA, Kelly K. 2014. Twenty years post-NIH revitalization act: Enhancing minority participation in clinical trials (EMPaCT): Laying the groundwork for improving minority clinical trial accrual: Renewing the case for enhancing minority participation in cancer clinical trials. Cancer 120 Suppl 7(0):1091-6.

Chinn JJ, Martin IK, Redmond N. 2021. Health equity among black women in the united states. Journal of Women's Health 30(2):212-9. http://doi.org/10.1089/jwh.2020.8868

Collins MD, Hoyles L, Törnqvist E, von Essen R, Falsen E. 2001. Characterization of some strains from human clinical sources which resemble “Leptotrichia sanguinegens”: Description of sneathia sanguinegens sp. nov., gen. nov. Syst Appl Microbiol 24(3):358-61.

Duployez C, Le Guern R, Faure E, Wallet F, Loïez C. 2020. Sneathia amnii, an unusual pathogen in spondylitis: A case report. Anaerobe 66:102277. https://doi.org/10.1016/j.anaerobe.2020.102277

Fettweis JM, Brooks JP, Serrano MG, Sheth NU, Girerd PH, Edwards DJ, Strauss JF, The Vaginal MC, Jefferson KK, Buck GA. 2014. Differences in vaginal microbiome in african american women versus women of european ancestry. Microbiology 160:2272-82.

Fettweis JM, Serrano MG, Paul BJ, Edwards DJ, Girerd PH, Parikh HI, Huang B, Arodz TJ, Edupuganti Laahirie, Glascock AL, et al. 2019. The vaginal microbiome and preterm birth. Nature Medicine. 25(6):1012-21. DOI:10.1038/s41591-019-0450-2.

Gentile GL, Rupert AS, Carrasco LI, Garcia EM, Kumar NG, Walsh SW, Jefferson KK. 2020. Identification of a cytopathogenic toxin from sneathia amnii. J Bacteriol 202(13):162. https://jb.asm.org/content/202/13/e00162-20.

Giurgescu C, Banks A, Dancy BL, Norr K. 2013. African american women's views of factors impacting preterm birth. MCN.the American Journal of Maternal Child Nursing 38(4):229-34.

Goldenberg RL, Hauth JC, Andrews WW. 2000. Intrauterine infection and preterm delivery. N Engl J Med 342(20):1500-7.

Han YW, Shen T, Chung P, Buhimschi IA, Buhimschi CS. 2009. Uncultivated bacteria as etiologic agents of intra-amniotic inflammation leading to preterm birth. J Clin Microbiol. 47(1):38-47. doi: 10.1128/JCM.01206-08.

Harwich MD, Serrano MG, Fettweis JM, Alves JMP, Reimers MA, Buck GA, Jefferson KK, Vaginal Microbiome Consortium (additional members). 2012. Genomic sequence analysis and characterization of sneathia amnii sp. nov. BMC Genomics 13(8):S4. https://doi.org/10.1186/1471-2164-13-S8-S4.

Jefferson KK. 2012. The bacterial etiology of preterm birth. Adv Appl Microbiol. 80:1-22. doi: 10.1016/B978-0-12-394381-1.00001-5.

Koumans EH, Sternberg M, Bruce C, McQuillan G, Kendrick J, Sutton M, Markowitz LE. 2007. The prevalence of bacterial vaginosis in the United States, 2001–2004; associations with symptoms, sexual behaviors, and reproductive health. Sex Transm Dis 34(11):864-869. doi: 10.1097/OLQ.0b013e318074e565.

LaVallie ER, DiBlasio EA, Kovacic S, Grant KL, Schendel PF, McCoy JM. 1993. Bio/Technology. 11, 187–193.

Mazar J and Cotter PA. 2007. New insight into the molecular mechanisms of two-partner secretion. Trends Microbiol 15(11):508-15. https://doi.org/10.1016/j.tim.2007.10.005

Vaneechoutte M. 2017. Lactobacillus iners, the unusual suspect. Res Microbiol 168(9):826-36.

Verstraelen H, Verhelst R, Claeys G, De Backer E, Temmerman M, Vaneechoutte M. 2009. Longitudinal analysis of the vaginal microflora in pregnancy suggests that L. crispatus promotes the stability of the normal vaginal microflora and that L. gasseri and/or L. iners are more conducive to the occurrence of abnormal vaginal microflora. BMC Microbiology 9:116.

Walani SR. 2020. Global burden of preterm birth. Int J Gynecol Obstet 150(1):31-3.